Artefacts of Finite-Span Domain in Vortex-Induced Vibration Simulations

Xingeng Wu[1], Anupam Sharma[2,*]

Department of Aerospace Engineering, Iowa State University, Ames, Iowa, 50011

Abstract

The effects of finite-span computational domain with periodic boundaries for vortex-induced vibration simulations are investigated. Coupled fluid-solid dynamics of an elastically-mounted rigid circular cylinder are performed using detached eddy simulations with four computational domains of varying span lengths. Simulations with span less than five cylinder diameters give erroneous results. Spectra of integrated transverse loading and spanwise coherence of sectional force coefficient are analyzed to explain the observations.

1. Introduction

Vortex-induced vibration (VIV) is commonly observed in bridge decks, cables, power conductors, risers in oil rigs, etc. The Kármán vortex shedding in the wake of a bluff body causes periodic forcing on the body. In certain conditions the vortex-shedding frequency synchronizes ("lock-in") with the natural frequency of the system which results in high-amplitude oscillations limited only by the system damping. Experimental investigations of VIV are typically performed with finite-span cylinders with aspect ratios of around 10 to minimize "end effects"(e.g, Govardhan and Williamson [1]), where "end-effects" refers to effects due to three-dimensional flow at span ends. End plates have been used in experiments (e.g., Morse et al. [2]), which reduce but not completely eliminate the end effects.

This problem is avoided in simulations by using periodic boundaries in the span direction. While the periodic boundaries imply an infinitely-long cylinder, the finite size of the computational domain in the span direction imposes artificial periodicity in the flow. If spanwise variations are present in the flow and the length scale of these variations is larger than the simulated span, then span periodicity can yield incorrect results. For a turbulent flow, this length scale can be measured using two-point correlations; in particular, spanwise coherence. Magnitude-squared coherence is defined as $\gamma^2(\Delta z, f) = \langle |S_{xy}(f)|^2 \rangle / (\langle S_{xx}(f) \rangle \langle S_{yy}(f) \rangle)$, where $S_{xy}(f)$ denotes cross-spectral density of the desired quantity (e.g., sectional force) at points $\boldsymbol{x}$ and $\boldsymbol{y}$ separated by a distance Δz along the span, $S_{xx}(f)$ and $S_{yy}(f)$ are auto-spectral densities at $\boldsymbol{x}$ and $\boldsymbol{y}$ respectively, and angle brackets denote ensemble averaging.

Figure 1 presents contours of γ^2 of sectional transverse force for a static circular cylinder (aspect ratio, L/D=20) simulation. Nondimensional frequency, $k = f\,D/V_\infty$ is used here to plot coherence which is small everywhere except at the Kármán vortex-shedding frequency, f_v. The Strouhal number, $St = f_v D/V_\infty$ is ~ 0.2. Several studies (e.g. Labbé and Wilson [3]) have investigated the impact of span length in simulations of flow over *stationary* cylinders.

*Corresponding author

Email address: sharma@iastate.edu (Anupam Sharma)

[1]Graduate Student

[2]Associate Professor, Iowa State University

In this paper, we investigate the effect of domain size when simulating VIV of a circular cylinder with periodic boundaries in the span direction. While the effect of finite span (aspect ratio or span length-to-diameter ratio, L/D) on VIV has been investigated experimentally (e.g., Szepessy and Bearman [4]), such an investigation is lacking for simulations. Although Lucor et al. [5] analyzed spanwise correlation in their VIV simulations of one cylinder with $L/D = 26$, they did not investigate the impact of varying L/D. We present detached eddy simulation results of VIV of four models with $L/D = 1,\ 2,\ 5$, and 10. Displacement amplitude, oscillation frequency, lift spectra, and spanwise coherence are compared between the simulations.

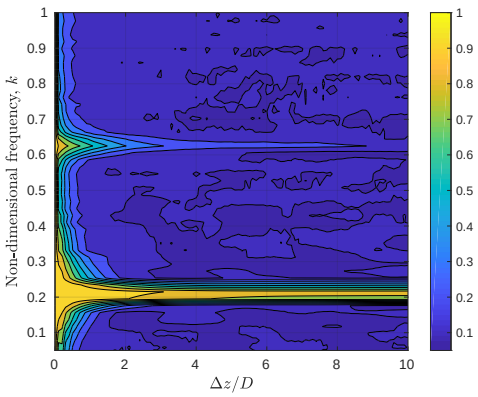

Figure 1: $\gamma^2(\Delta z, f)$ for a static cylinder

2. Computational Methodology and Verification

A coupled fluid-solid dynamics solver is used to simulate an elastically-mounted rigid circular cylinder experiencing VIV. A k-ω detached eddy simulation (DES) technique [6] is used to model the flow and a forced single degree of freedom mass-spring-damper system is solved to model the dynamics of the cylinder. The details are provided in Wu *et al.* [7].

Figure 2 shows a schematic of the simulation setup and comparisons with measured data from Ref. [8] for a low mass-damping cylinder undergoing VIV. The following nondimensional numbers are matched between the experiment and the simulations: mass ratio, $m^* = 2.6$, mechanical damping ratio, $\zeta = 0.001$, and reduced velocity, $V_R = V_\infty/(f_N D)$, where f_N is the natural frequency of the system. The flow Reynolds number based on the cylinder diameter, $Re_D = 2 \times 10^4$. The same values of m^*, ζ, and Re_D are used for all the simulations in the paper.

The simulations accurately predict the displacement amplitude and the vortex shedding frequency of the cylinder (see Fig. 2) over a wide range of V_R which includes the four branches identified in Ref. [8]: *Initial Excitation*, *Upper*, *Lower*, and *Desynchronization*. Of particular interest is the "lock-in" phenomenon which occurs in the *Upper* and *Lower* branches where the chances of structural damage are highest.

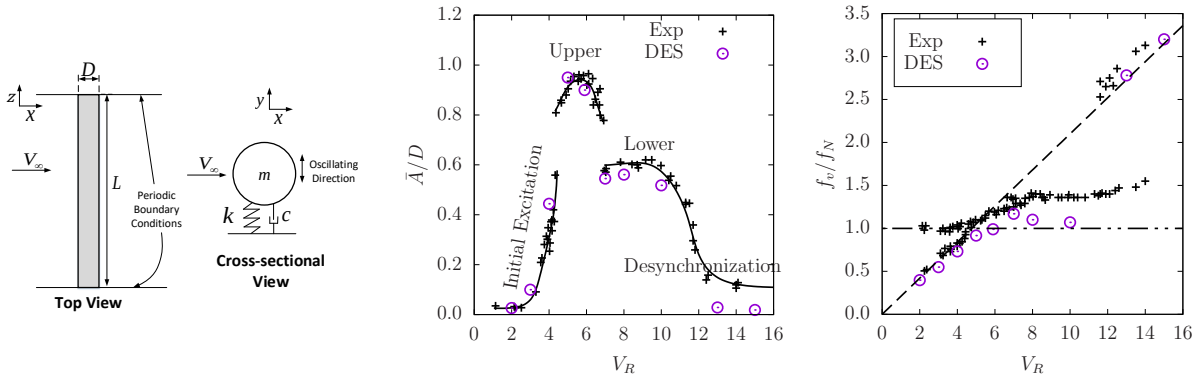

(a) simulation setup (b) mean amplitude (c) frequency

Figure 2: Verification of the DES approach to predict VIV: (a) a schematic showing the simulation setup, (b) mean nondimensional displacement amplitude ($\bar{A}/D$), and (c) normalized oscillation frequency (f_v/f_N). Measured data is from Ref. [8].

3. Effect of Aspect Ratio

Four cylinder models with aspect ratio, $L/D = 1, 2, 5$, and 10 are modeled. For each configuration, seven values of reduced velocity V_R $(= 2, 3, 4, 5, 5.9, 7, 8)$ are evaluated; this wide range of V_R covers the *Initial Excitation*, *Upper*, and *Lower* branches. Figure 3 compares the predicted scaled mean amplitude $(\bar{A}/D)$ and the normalized oscillation frequency (f_v/f_N) for the different models. The convergence of the results for models with $L/D = 5$ and 10 shows that span length of $10\,D$ is adequate for VIV simulations. While the smaller-span models exhibit the same qualitative trend, moderate-to-large differences are observed between them in the *Initial Excitation* and *Upper* branches including underprediction of the peak amplitude.

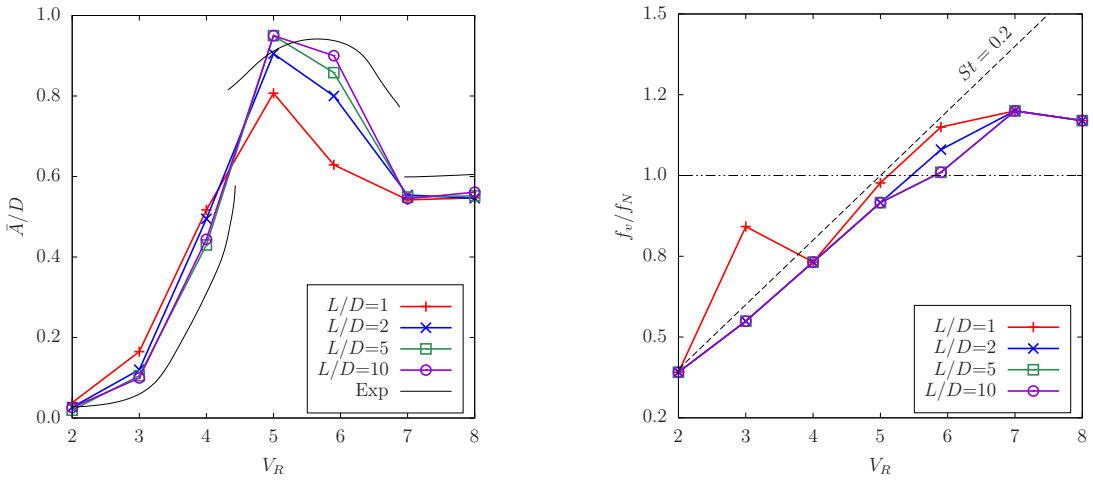

(a) mean amplitude (b) frequency

Figure 3: Comparison of predicted (a) $\bar{A}/D$, and (b) normalized oscillation frequency, using cylinder models of different span lengths.

3.1. $V_R = 5$

Peak amplitude is observed when f_v matches f_N (resonance condition). The k corresponding to f_N is called k_N $(= 1/V_R = 0.2$ for $V_R = 5)$. Power spectral density (PSD) of the transverse aerodynamic force coefficient, $C_y = 2F_y/(\rho V_\infty^2 L)$ of the four models are compared in Fig. 4 (a). A linear scale is used to plot the PSDs to accentuate the differences. The spectral peak is higher and narrower for the models with $L \geq 5D$. For shorter-span models, the energy is distributed over a wider frequency range, resulting in a broader peak. A sharp peak in C_y at $k \sim St$ results in greater excitation, hence higher $\bar{A}/D$, for the larger-span models at $V_R = 5$.

Spanwise coherence of transverse sectional force coefficient, $c_y(z) = 2f_y(z)/(\rho V_\infty^2)$ are plotted in Fig. 4 (b) for $V_R = 5$. For the larger-span cylinders $(L \geq 5D)$, high coherence (γ^2) is limited to a very small band of k around St (~ 0.2), whereas for the smaller-span models, γ^2 is very high over the entire span for $0.1 < k < 0.3$. High coherence at frequencies away from $k = St$ is the reason for the broader but shorter peaks observed in the C_y spectra for the smaller-span models.

3.2. $V_R = 5.9$

Smaller-span models underpredict $\bar{A}/D$ throughout the *Upper* branch. The solutions at $V_R = 5.9$ are probed to investigate this underprediction. Figure 5 plots the C_y spectra and the spanwise coherence of c_y for the different models. The k corresponding to the natural frequency is $k_N = 1/V_R \sim 0.17$ for $V_R = 5.9$. The C_y spectra for the small-span models peak at $k \sim 0.2$ and "lock-in" with k_N does not occur. The spectrum of the largest-span model peaks around k_N; the peak is not exactly at k_N due to the added-mass effect, which can be substantial for

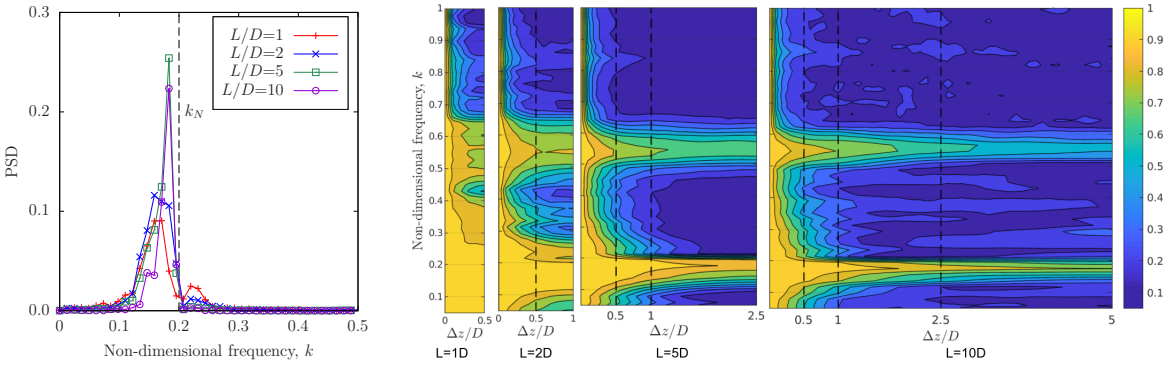

(a) C_y spectra (b) coherence of c_y

Figure 4: Results for V_R=5: (a) PSD of C_y, and (b) $\gamma^2(\Delta z, k)$ of c_y for models with L/D=1,2,5,&10.

low-m^* systems. High coherence in the small-span models forces the vortex shedding at $k \sim 0.2$ and does not allow "lock-in" at k_N.

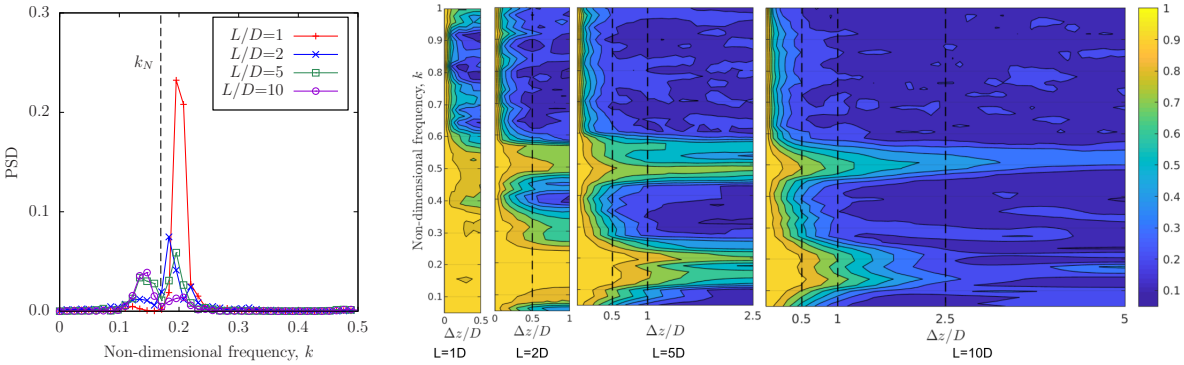

(a) C_y spectra (b) coherence of c_y

Figure 5: Results for V_R=5.9: (a) PSD of C_y, and (b) $\gamma^2(\Delta z, k)$ of c_y for models with L/D=1,2,5,&10.

3.3. $V_R = 3$

In contrast to underprediction in the "lock-in" region, the smaller-span models overpredict $\bar{A}/D$ in the *Initial Excitation* branch. This is consistent with the C_y spectra which shows a higher peak at $k \sim 0.2$ for the smaller-span models (see Fig. 6 (a)). Another peak is observed with the smaller-span models at k near k_N (~ 0.33 for $V_R = 3$). Figure 6 (b) shows increased coherence at k_N. The periodicity in smaller span models reinforces the excitation at this frequency leading to the additional peak in the C_y spectra. In fact, the smallest-span model oscillates at this frequency (see Fig. 3 (b)), suggesting a "lock-in" in the *Initial Excitation* branch.

4. Conclusion

DES of VIV of an elastically-mounted rigid circular cylinder are performed with periodic boundaries for four domains with span L = 1-,2-,5-, and 10 D. The results show that a minimum span of 5 D is required to accurately predict VIV. Simulations with smaller-span domains underpredict the peak displacement amplitude and give erroneous predictions of the "lock-in" frequencies. High spanwise coherence in these models at frequencies other than the vortex-shedding frequency is responsible for the observed artefacts.

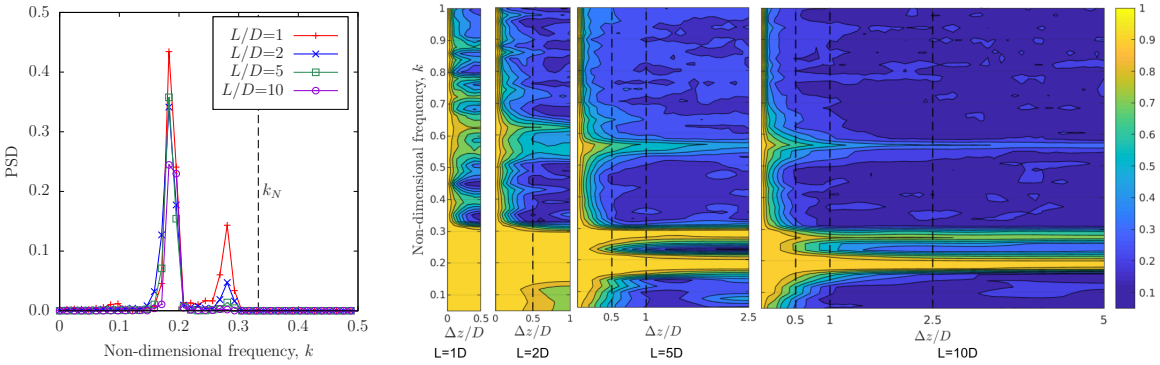

(a) C_y spectra (b) coherence of c_y

Figure 6: Results for V_R=3: (a) PSD of C_y, and (b) $\gamma^2(\Delta z, k)$ of c_y for models with L/D=1,2,5,&10.

5. Acknowledgments

Funding for this research is provided by the National Science Foundation (Grant #NSF/ CMMI-1537917). Computational resources are provided by NSF XSEDE (Grant #TG-CTS130004) and by DOE ALCF.

References

1. Govardhan, R., Williamson, C. Critical mass in vortex-induced vibration of a cylinder. *European Journal of Mechanics-B/Fluids* 2004;**23**(1):17–27.

2. Morse, T., Govardhan, R., Williamson, C. The effect of end conditions on the vortex-induced vibration of cylinders. *Journal of Fluids and Structures* 2008;**24**(8):1227–1239.

3. Labbé, D., Wilson, P. A numerical investigation of the effects of the spanwise length on the 3-d wake of a circular cylinder. *Journal of Fluids and Structures* 2007;**23**(8):1168–1188.

4. Szepessy, S., Bearman, P. Aspect ratio and end plate effects on vortex shedding from a circular cylinder. *Journal of Fluid Mechanics* 1992;**234**:191–217.

5. Lucor, D., Foo, J., Karniadakis, G. Vortex mode selection of a rigid cylinder subject to viv at low mass-damping. *Journal of Fluids and Structures* 2005;**20**(4):483–503.

6. Yin, Z., Reddy, K., Durbin, P.A. On the dynamic computation of the model constant in delayed detached eddy simulation. *Physics of Fluids* 2015;**27**(2).

7. Wu, X., Jafari, M., Sarkar, P., Sharma, A. Verification of des for flow over rigidly and elastically-mounted circular cylinders in normal and yawed flow. *Journal of Fluids and Structures* 2019; (under review).

8. Khalak, A., Williamson, C. Fluid forces and dynamics of a hydroelastic structure with very low mass and damping. *Journal of Fluids and Structures* 1997;**11**(8):973–982.